PLUNGER LIFT STATE IDENTIFICATION & POB METHODOLOGY USING HIGH-RESOLUTION SURFACE DATA

SLUG-BASED EFFICIENCY ESTIMATION, HEALTH MONITORING, AND MACHINE LEARNING INTEGRATION

Louie Cruz, Malek Rekik, and Egidio (Ed) Marotta
SLB

Abstract

Plunger lift systems experience cyclic transitions between shut-in buildup and flow periods, during which surface pressure responses reflect subsurface liquid accumulation, gas compression, and mechanical plunger motion. While operational deviations may be visually apparent in production data, identifying root cause often requires discrimination between mechanical malfunction, hydraulic retention loss, and reservoir-driven behavior.

This paper presents a structured methodology for statistical state identification and cycle-level slug efficiency estimation using high-frequency (1-second) surface pressure data. An inferred accumulated slug proxy is derived from peak shut-in differential pressure and delivered slug volume is estimated from arrival velocity and slug duration. A relative lift efficiency index is computed on a cycle-by-cycle basis.

A field case study demonstrates diagnosis of standing valve failure through collapse of shut-in differential pressure and degradation of lift efficiency while plunger roundtrip motion persisted. The framework provides a physics-informed artificial intelligence foundation for integration with outer-loop statistical and machine learning approaches for anomaly detection and adaptive optimization.

I. Introduction

Plunger lift is a widely deployed artificial lift method for unloading liquid from gas wells operating at declining reservoir energy [1], [2]. The system operates cyclically: during shut-in, gas pressure builds in the annulus while liquid accumulates above the plunger in the tubing; during opening, the stored energy lifts the accumulated slug to surface.

The hydrostatic contribution of a liquid column is governed by:

$$\Delta P = \rho g h \ (1)$$

where ΔP represents hydrostatic pressure, ρ fluid density, g gravitational acceleration, and h liquid column height. This relationship forms the basis for estimating hydrostatic pressure gradients in vertical wellbores and is widely used in petroleum production engineering to relate pressure measurements to fluid column height [3], [4].

Under normal operation, peak shut-in casing and tubing pressures define the retained hydraulic energy available for the subsequent lift cycle. In field operations, these pressure relationships are commonly used by operators to infer whether sufficient liquid has accumulated to justify opening the well for a lift cycle.

However, degradation of mechanical components such as standing valves can disrupt liquid retention while allowing plunger travel to continue[5]. In such cases, production decline may occur without obvious non-arrival behavior.

Traditional plunger lift control relies on threshold-based triggers and arrival sensing [1], [2]. While effective for basic cycling, these approaches do not fully exploit high-frequency pressure data for structured diagnostic inference.

This paper formalizes a deterministic, physics-based framework for:

1. Cycle-level state identification
2. Slug accumulation estimation
3. Delivered slug inference
4. Relative lift efficiency computation
5. Discrimination between hydraulic retention failure and mechanical non-arrivals

The methodology is compatible with marginal-well economics and scalable toward data-driven extensions.

II. High-Frequency Feature Extraction

Shut-In Peak Tracking:

During each shut-in period, peak casing and tubing pressures are recorded:

$$CP\_\max \ (2)$$
$$TP\_\max \ (3)$$

The shut-in differential pressure is defined:

$$\Delta P\_close = CP\_max - TP\_\max \quad (4)$$

Peak values are reset at the beginning of each closed cycle to maintain statistical independence between cycles. Differential pressure during shut-in serves as a practical indicator of retained hydrostatic load within the tubing column [3].

Load Factor:
A normalized load factor is computed as:

$$Load\ Factor = \frac{(CP - TP)}{(CP - LP)} \times 100 \quad (5)$$

where LP is line pressure.

This dimensionless metric normalizes casing-to-tubing differential relative to available drawdown. Load-based normalization concepts have precedent in gas lift and artificial lift performance evaluation [5].

III. Slug Accumulation and Delivery Estimation

Accumulated Slug Proxy:

During the shut-in period of a plunger lift cycle, liquid accumulates in the tubing above the plunger while gas pressure builds within the casing. The resulting hydrostatic column contributes to the differential pressure measured between casing and tubing near the end of the shut-in interval.

A relative proxy for accumulated liquid load can therefore be expressed as

$$V_{accum} \propto \Delta P_{close} \cdot D_{eff}^2 \quad (6)$$

where D_{eff} represents the effective hydraulic diameter of the tubing.
This formulation follows directly from the hydrostatic relation in Eq. (1). In practice, the calculation assumes a representative liquid gradient consistent with common multiphase flow approximations used in production engineering [4].
Because actual wellbore conditions may include gas entrainment, changing liquid density, or transient multiphase flow, the resulting value should be interpreted as a relative indicator of accumulated hydraulic load rather than an absolute volumetric measurement.
When evaluated across multiple cycles within the same well, the metric provides a consistent basis for comparing relative liquid accumulation behavior and identifying changes in well loading trends that may require adjustment of cycle timing or control parameters.

Arrival Detection and Kinematic Inference:
Arrival duration is defined as elapsed time between valve opening and confirmed plunger arrival. Arrival velocity can be estimated as,

$$v_{arr} = \frac{MD}{t_{arr}} \quad (7).$$

Velocity-based arrival inference is consistent with established plunger lift performance models and provides a practical approximation of plunger dynamics under typical operating conditions [1], [6].

Delivered Slug Volume:
Delivered slug volume can be estimated using,

$$V_{delivered} \approx A \cdot v_{arr} \cdot t_{slug} \quad (8)$$

where *A* is tubing cross-sectional area and t_{slug} is slug duration.

This represents a simplified kinematic approximation of liquid displacement during the plunger ascent phase. Multiphase effects such as gas-liquid slip, fallback, or transient flow regimes may influence the relationship between slug duration and actual delivered liquid volume. [4].

Lift Efficiency Index:
Relative lift efficiency can be defined as,

$$\eta_{lift} = \frac{V_{delivered}}{V_{accum}} \, x \, 100 \quad (9)$$

This dimensionless index provides cycle-to-cycle performance comparison. Cycles lacking confirmed slug onset or arrival are excluded.

IV. Case Study: Standing Valve Failure

A vertical natural gas well exhibited stable cycling characterized by repeatable ΔP_{close} and consistent arrival velocity.
An clear operational deviation was observed when:

- Tubing pressure increases during shut-in
- ΔP_{close} collapses
- Delivered slug volume decreases
- Lift efficiency degrades
- Plunger arrival continues

Loss of hydraulic isolation below the plunger is consistent with standing valve failure, allowing fluid evacuation during plunger descent [6],[7].

The collapse of ΔP during close combined with degradation of η_{lift} enables rapid discrimination between hydraulic retention failure and mechanical non-arrival. Following valve replacement, differential pressure and efficiency returned to baseline.

V. Discussion

The integration of shut-in peak tracking, differential-pressure slug inference, kinematic delivery estimation, and relative efficiency indexing provides layered diagnostic capability for plunger lift systems.

By structuring high-frequency pressure measurements at the level of individual plunger cycles, raw time-series data are converted into interpretable indicators describing hydraulic loading, plunger dynamics, and liquid delivery performance.

The differential pressure ΔP during close represents a practical proxy for retained hydraulic energy within the tubing. While not a direct volumetric measurement, the differential pressure provides a consistent indicator of liquid accumulation when interpreted within the operational context of the well.

Delivered slug estimates derived from plunger arrival velocity and slug duration provide a complementary observation of actual lift performance during each cycle.

In field applications, cycles exhibiting both high retained load and high delivery efficiency typically represent stable plunger lift operation where accumulated liquid is consistently removed from the wellbore.

Cycles that retain substantial load but exhibit poor delivery may indicate plunger bypass, fallback, or increased drag during ascent. Conversely, simultaneous collapse of retained load and delivery efficiency while plunger round-trip motion continues is consistent with hydraulic isolation failure such as standing valve leakage.

Structured cycle-level features derived from this framework provide well-defined inputs for statistical change-point detection [8], [9] and anomaly detection methods [10].

VI. Physics & Data Science Modeling

Introduction:

Accurate detection of plunger arrival at bottom is a critical component of modern plunger lift optimization [6]. Reliable identification of on-bottom events directly affects cycle timing, liquid unloading efficiency, gas production stability, and long-term equipment health monitoring. Inaccurate or missed detections can lead to improper shut-in timing, inefficient lift cycles, increased wear, and suboptimal well performance.

Historically, on-bottom detection has relied on statistical identification of a small transient pressure disturbance observed in tubing pressure measurements. This disturbance corresponds to the pressure wave generated when the descending plunger impacts the bottom bumper spring and propagates to the surface sensor [5]. While this approach can be effective under ideal conditions, it suffers from significant limitations. The pressure blip may be weak, masked by noise, distorted by gas interference, or entirely absent depending on well conditions. As a result, statistical detection methods often require frequent manual tuning and subject matter expert oversight, particularly as wells age or operating conditions change.

With the introduction of the Smarten Unify™ plunger lift control system, capable of collecting and transmitting 1-second surface pressure data to the cloud, new opportunities emerged for more advanced analytics. However, the controller is based on an ESP32 embedded

platform with constrained computational resources, limited memory, and no capability for deploying computationally intensive machine learning models. This constraint fundamentally shaped the algorithmic design strategy. Rather than deploying a fully data-driven model at the edge, a hybrid architecture was developed that separates lightweight real-time physics-based estimation in the controller from computationally intensive probabilistic inference in the cloud.

The online component embedded in the controller integrates a reduced-order dynamic model of plunger descent in real time. Using tubing pressure measurements and a small set of lumped coefficients representing friction and drag effects, the model numerically integrates Newton's second law to estimate plunger position and velocity at each sampling interval. On-bottom detection is therefore determined by the simulated plunger reaching known tubing depth, rather than by detecting a transient pressure disturbance. This physics-based formulation inherently filters high-frequency pressure noise and remains functional even when the traditional pressure blip is weak or absent.

Because well conditions evolve over time due to plunger wear, tubing scaling, and reservoir pressure depletion, static model parameters would eventually drift, and thus, degrade accuracy. To address this, an offline cloud-based adaptation layer was developed. The cloud process analyzes each plunger drop cycle using Bayesian change point detection techniques [9] to probabilistically estimate true on-bottom timing from pressure data. These labeled cycles are then used to periodically re-optimize the online model coefficients using Bayesian optimization [11]. Updated parameters are subsequently pushed to the controller, enabling gradual adaptation while preserving real-time computational efficiency.

The resulting edge-cloud architecture leverages the strengths of both environments: deterministic, low-cost physics-based estimation at the controller level and probabilistic inference with uncertainty quantification in the cloud. The system is currently deployed on more than 900 wells and has been validated on 50 wells, demonstrating approximately 95% on-bottom detection accuracy compared to approximately 50% accuracy using traditional statistical detection methods, which require continuous tuning. By shifting from transient feature detection to dynamic state estimation, the proposed approach improves robustness, reduces operational oversight, HSE enhancements, and enables additional health monitoring insights through long-term tracking of friction-related model coefficients.

The following sections describe the online dynamic model formulation, the offline Bayesian labeling framework, the parameter adaptation strategy, and field validation results.

1.1 Problem Definition and Design Constraints:

- Operational Definition of On-Bottom

  On bottom is defined as the moment the descending plunger mechanically impacts the bottom bumper spring at tubing depth. This event determines cycle timing and directly affects unloading efficiency and well performance.

  The event occurs downhole and is not directly measurable. Surface detection relies primarily on tubing pressure, where impact is expected to generate a pressure

disturbance that travels to the sensor. However, the surface signature is indirect and condition dependent.

2.2 Limitations of Statistical Detection

- Traditional detection identifies a small transient “blip” in tubing pressure. This method has key limitations:
  - The blip may be absent or attenuated.
  - It is sensitive to noise and transient fluctuations.
  - Parameters do not generalize well across wells.
  - Frequent manual tuning is required as conditions change.

As a result, detection reliability degrades over time and scalability is limited.

2.3 Embedded Hardware Constraints

The Smarten Unify controller operates on an ESP32 platform with 1-second sampling. Computational resources and memory are limited, and real-time deterministic execution is required.

Heavy machine learning models and iterative inference algorithms are not suitable for embedded deployment. Each pressure update must be processed with minimal and predictable computational cost.

These operational and hardware constraints motivated a hybrid architecture combining lightweight real-time physics-based estimation at the controller with cloud-based probabilistic adaptation.

Hybrid Architecture Overview:

The proposed solution adopts a hybrid edge–cloud architecture that separates real-time deterministic estimation from computationally intensive validation and adaptation as shown in Figure 1. The online component resides within the Smarten Unify controller and executes a lightweight physics-based model at a 1-second sampling rate using surface pressure measurements. This embedded model continuously estimates plunger position and determines on-bottom arrival based on simulated dynamics.

Simultaneously, pressure and cycle data are transmitted to the cloud for offline processing. The cloud layer performs probabilistic validation, change-point analysis/ detection, and parameter optimization using more advanced statistical and machine learning techniques. Updated model coefficients are then periodically pushed back to the controller, enabling gradual adaptation without increasing embedded computational complexity.

This architecture leverages the strengths of both environments: deterministic, low-latency estimation at the edge and scalable probabilistic inference in the cloud. The result is a robust and adaptive on-bottom detection system suitable for large-scale deployment.

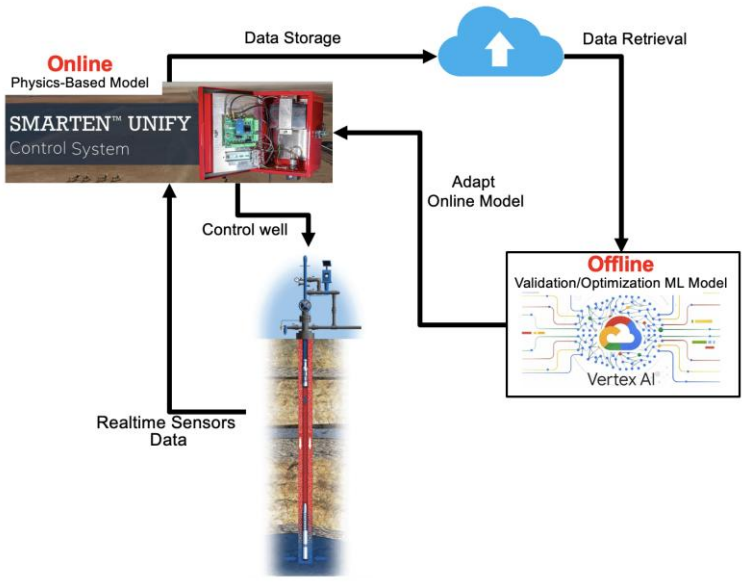

Figure 1. Hybrid edge–cloud architecture for real-time physics-based on-bottom detection and cloud-based adaptive optimization. Source: SLB

Online Model - Physics Based Approach:

The online model is implemented directly within the Smarten Unify controller and operates at a fixed 1-second sampling interval. Instead of detecting a transient pressure disturbance, the approach estimates plunger dynamics in real time using a reduced-order physical model. At release, initial conditions are set and the plunger position is updated sequentially using tubing pressure measurements as the primary driving input.

At each time-step, Newton's second law is applied in discrete form. The net force acting on the plunger, driven by pressure differential and opposed by lumped friction and drag terms, is integrated numerically using a second-order Taylor approximation such that

$$X_t = f(P_C, P_T, X_{t-1}, X_{t-2}) \quad (10)$$

where P_C is the casing pressure, P_T is the tubing pressure and X_t is the estimated plunger position at time t. This produces a recursive update of plunger position based on previous states and current pressure readings. The computational load is minimal, requiring only a deterministic state update per sample.

On-bottom is declared when the estimated plunger position reaches the known tubing depth as shown in Figure 2. Because detection is based on simulated descent rather than a pressure blip, the method remains functional even when the surface disturbance is weak or absent. Additionally, the dynamic formulation inherently filters high-frequency pressure noise, improving robustness compared to statistical threshold-based methods.

The model contains three lumped coefficients representing effective friction and drag characteristics of the well–plunger system. These coefficients influence descent velocity and are physically interpretable in terms of resistance magnitude. While simple in structure, the model provides continuous position and velocity estimates, enabling reliable on-bottom detection under varying operating conditions.

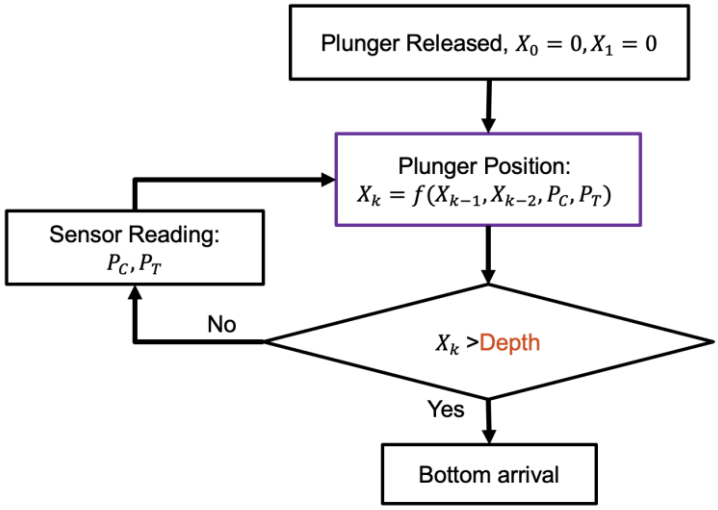

Figure 2. Real-time embedded plunger dynamics integration and on-bottom detection logic. Source: SLB

Offline Model - Validation, Optimization and Adaptation:

The offline workflow provides two functions: (i) probabilistic validation of on-bottom timing for individual cycles, and (ii) periodic adaptation of the online model coefficients using validated cycles. The process is executed cycle-by-cycle on cloud data and follows the same step order as the figures below.

Step 1: Restrict the search window:

As shown in Figure 3, for each drop cycle, the candidate on-bottom interval is constrained to a physically feasible window derived from descent-time bounds. This window is intentionally wide enough to cover operating variability, while restrictive enough to eliminate implausible early/late times and reduce false detections.

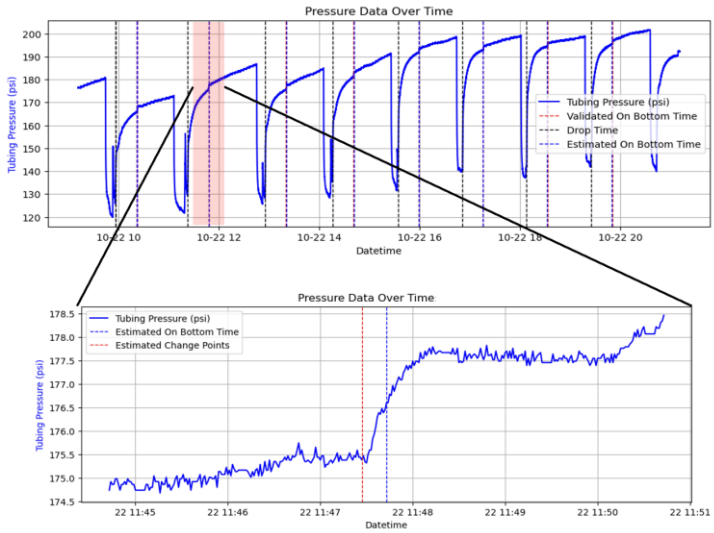

Figure 3. Example cycle showing tubing pressure response with validated and estimated on-bottom times and Bayesian change point detection zoom-in. Source: SLB

Step 2 - Local linear features and two-regime separation:

Within the candidate window, a moving linear fit is applied to the tubing-pressure trace, and the fitted parameters (e.g., slope/intercept) are stored as features such that

$$(m_k, b_k) = argmin_{m,b} \quad \Sigma_{i=1}^{n} \left(P_{T_i} - (m\, t_i + b) \right)^2 \quad (11)$$

where P_{T_i} is the tubing pressure measurement at time t_i within the moving window, t_i is the time stamp of the ith sample in the window, n is the number of samples in the moving window, m_k is the estimated local slope at window index k, b_k is the estimated local intercept at window index k, (m_k, b_k) are obtained by minimizing the sum of squared residuals between measured tubing pressure and the fitted local linear model within the window. These features are clustered into two regimes using k-means, representing behavior before and after on-bottom. The cluster centers are then used as representative local models for each regime as shown in Figure 4.

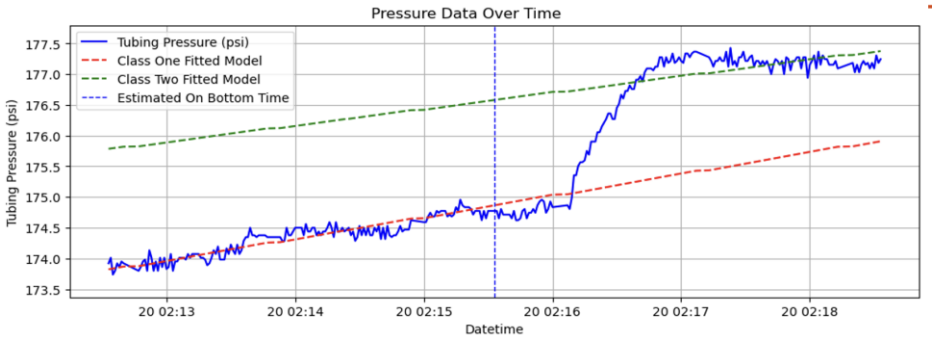

Figure 4. Local linear regime modeling and cluster-based separation around estimated on-bottom time. Source: SLB

Step 3 - Fuzzy membership transformation:

Because the regime transition can be noisy and k-means assignments may be locally inconsistent, the two representative regime models are converted into fuzzy membership functions. This maps the pressure signal into normalized regime-membership signals in [0,1] and it is determined as

$$\mu_j(t_i) = 1 - \frac{d\left(P_{T_i}, c_j(t_i)\right)^2}{\sum_{k=1}^{2} d\left(P_{T_i}, c_k(t_i)\right)^2} \in [0,1] \quad (12)$$

where P_{T_i} is the measured tubing pressure at time t_i, $c_j(t_i)$ is the jth representative regime model (cluster center line) evaluated at time t_i and $d(P_{T_i}, c_j(t_i))$ is the distance between the measured pressure and the jth regime model at that time (typically absolute or Euclidean distance). The denominator sums the squared distances to both regime models. $\mu_j(t_i)$ represents the fuzzy membership of the signal to regime j. The construction guarantees $\mu_j(t_i) \in [0,1]$ and $\mu_1(t_i) + \mu_2(t_i) = 1 \; \forall i$.

Two examples are shown: one with a clean regime transition as shown by Figure 5 below and one with a more ambiguous transition where multiple crossings occur as shown by Figure 6. This ambiguity is a key reason a probabilistic change point estimator is used rather than a single threshold crossing.

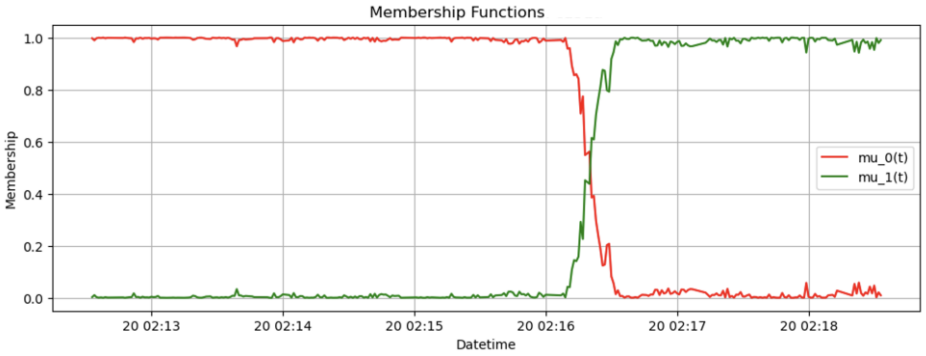

Figure 5. Fuzzy membership transformation of pressure signal for regime transition identification: Example 1. Source: SLB

Figure 6. Fuzzy membership transformation of pressure signal for regime transition identification: Example 2. Source: SLB

Step 4 - Bayesian change point estimation via MCMC:

A Bayesian change point model [11] is applied to the normalized membership signal, and Metropolis–Hastings MCMC [12] is used to sample plausible change point locations within the candidate window as shown in 7. This produces a distribution of change point candidates rather than a single point estimate.

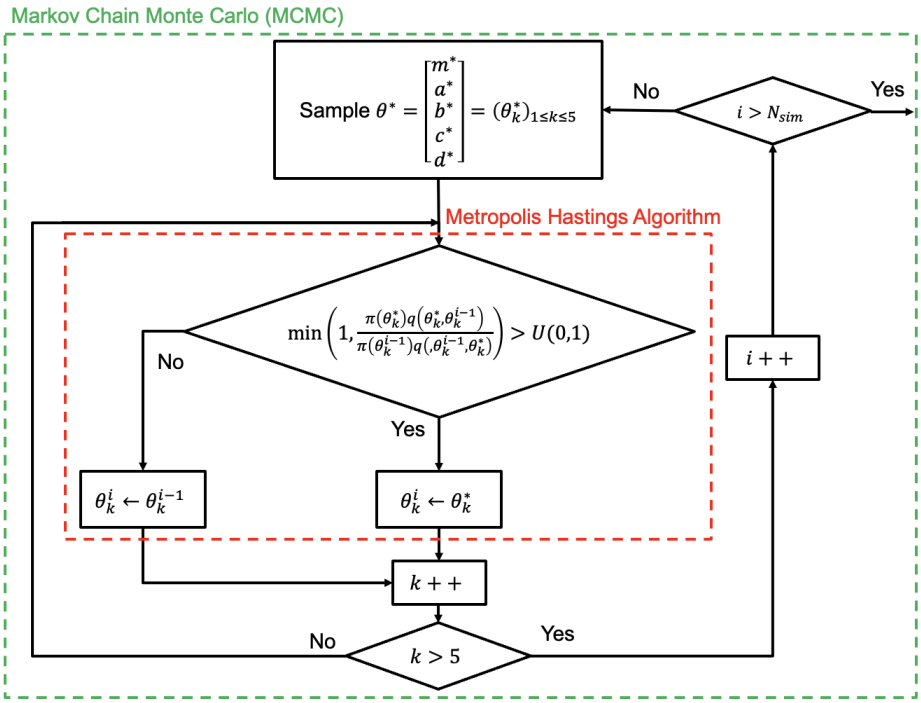

Figure 7. Metropolis–hastings MCMC framework for probabilistic change point estimation. Source: SLB

Step 5 - Cycle acceptance and labeling:

The sampled change point candidates define a posterior density. If the candidate spread meets the precision requirement (standard deviation ≤ 30 s), the *mean* of the distribution is accepted as the validated on-bottom time for that cycle. Otherwise, the cycle is rejected and excluded from subsequent optimization to avoid contaminating the parameter update with low-confidence labels. This is shown in Figure 8.

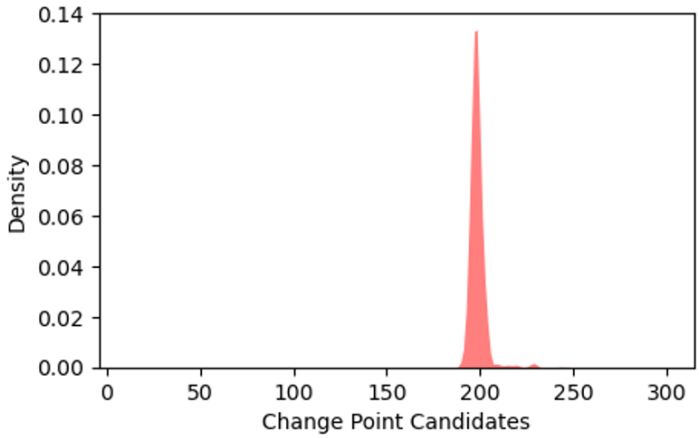

Figure 8. Posterior distribution of change point candidates from MCMC sampling. Source: SLB

Step 6 - Coefficient optimization and deployment:

Once a sufficient set of high-confidence cycles is labeled, the online physics-model coefficients are re-optimized offline by minimizing the position error evaluated at the validated on-bottom times such that

$$(a, b, c) = argmin_{a.b.c} \sum X\left(t_{validation_i}\right)^2 = argmin_{a.b.c} \sum E_i^2 \quad (13)$$

The updated coefficients are then pushed back to the controller on a periodic schedule, allowing gradual adaptation to changing well/plunger conditions while preserving deterministic real-time execution on the embedded device. This offline-to-online loop enables robust on-bottom labeling without manual tuning and provides controlled parameter drift over time, improving long-term reliability and scalability. An illustration of plunger release, descent dynamics, and on-bottom validation timing is shown in Figure 9.

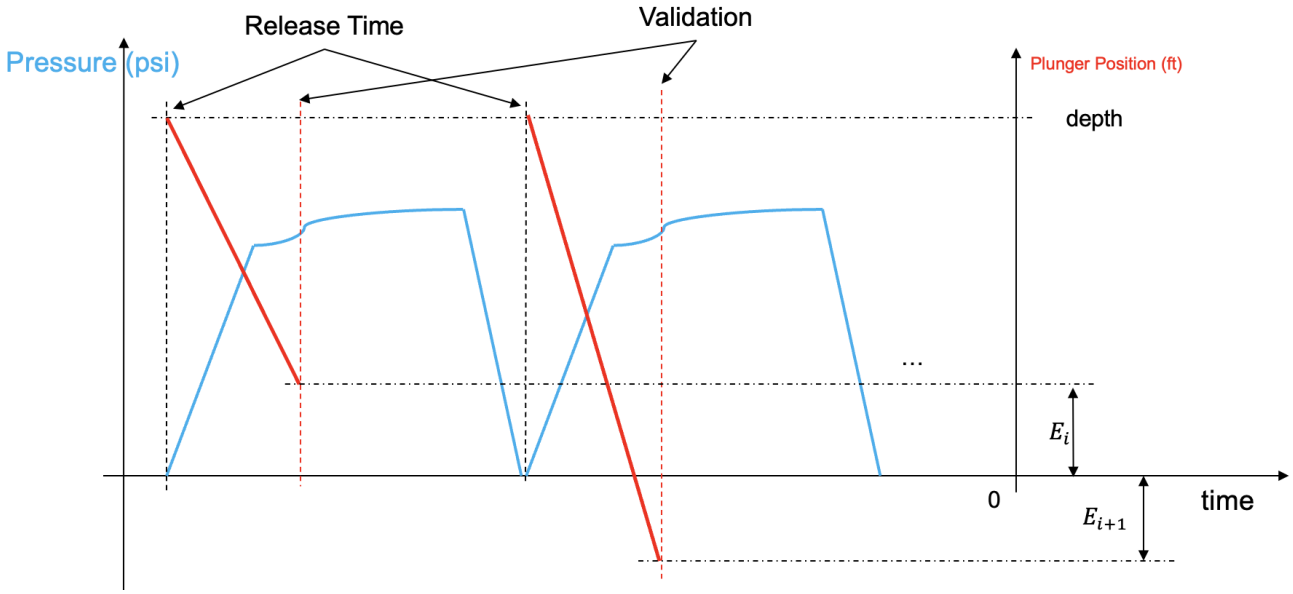

Figure 9. Conceptual illustration of plunger release, descent dynamics, and on-bottom validation timing. Source: SLB

Field Performance and Deployment Results:

The proposed hybrid system is currently deployed on more than 900 wells and was validated on a representative subset of 50 wells across varying operating conditions. Performance was evaluated against validated on-bottom times provided through SME manual review and operational records. Figure 10 illustrates a deployed well example showing surface pressures, plunger position estimation, and automated cycle state classification. The system consistently tracks descent dynamics and declares on-bottom without reliance on transient pressure blips.

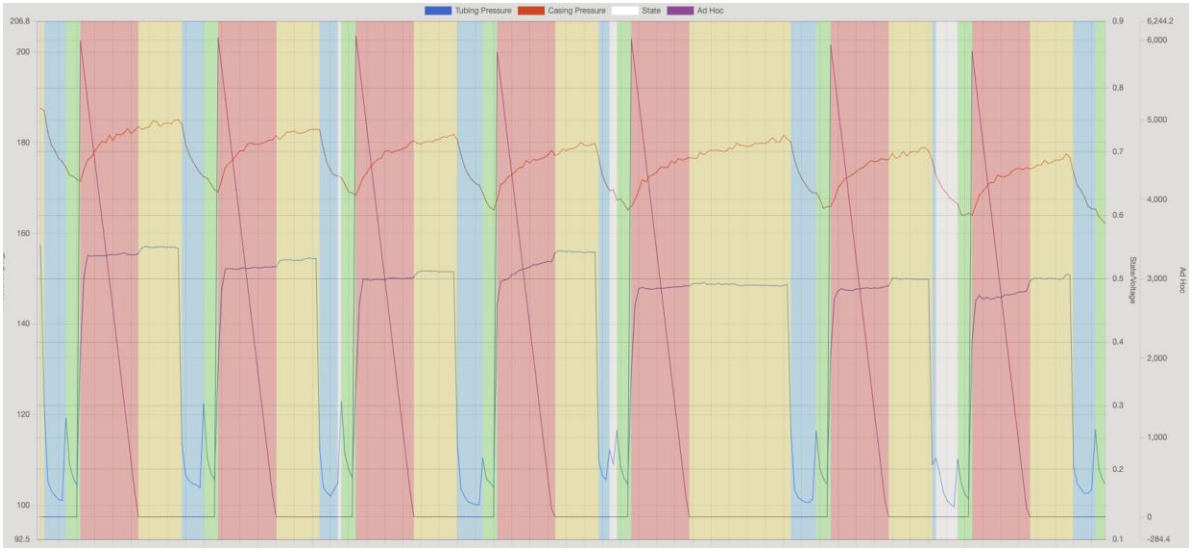

Figure 10. Deployed system visualization showing plunger position, surface pressures, and automated cycle state classification. Source: SLB

Figure 11 presents the distribution of the estimation error relative to validated on-bottom times. The majority of detections fall within ±30 seconds, meeting the defined precision requirement. Cycles failing the confidence threshold are excluded from parameter optimization; hence, preventing the degradation of the online model.

Table 1 compares performance against the conventional statistical method. The physics-based hybrid approach achieves 75% on-time detection within ±30 seconds and 99% within 2 minutes, with no undetected cycles, while significantly reducing early and false classifications. These results confirm that shifting from transient feature detection to physics-based state estimation combined with probabilistic validation improves robustness, scalability, and operational reliability across a large well populations.

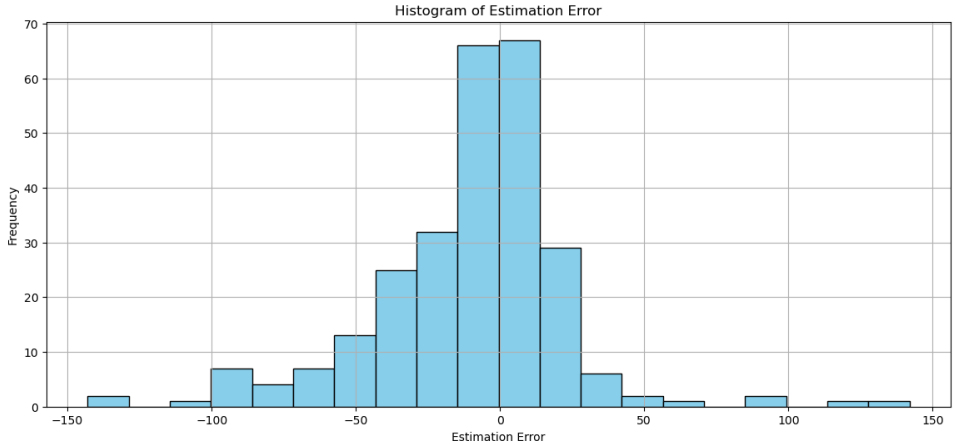

Figure 11. Histogram of on-bottom detection error relative to validated times showing majority of cycles within ±30 seconds. Source: SLB

Early	On time (+- 30 seconds)	Late	+- 1 minute	+- 2 minutes
21%	75%	4%	90%	99%

Table 1. Summary of on-bottom detection accuracy distribution showing 75% within ±30 seconds and 99% within ±2 minutes. Source: SLB

VII. Limitations

While the proposed framework provides a practical method for cycle-level diagnostic analysis of plunger lift systems, several limitations should be considered when interpreting the results.

The accumulated slug proxy derived from shut-in differential pressure represents a relative indicator of retained hydraulic load rather than a direct volumetric measurement. The formulation assumes a representative liquid gradient consistent with the hydrostatic relationship described in Eq. (1). In practice, the effective liquid gradient within the tubing may vary due to multiphase flow conditions, gas entrainment, or compositional differences in produced fluids.

Delivered slug estimation relies on simplified kinematic assumptions linking plunger velocity and slug duration to volumetric liquid transport. Real well conditions may include gas–liquid slip, fallback, and transient flow regimes that affect the relationship between measured slug duration and actual delivered liquid volume.

Sensor resolution and measurement reliability also influence the precision of cycle-level feature extraction. Pressure sensor drift, noise, or communication interruptions may affect the detection of peak pressures or timing events used in the diagnostic calculations.

Finally, the methodology is most applicable to conventional plunger lift systems where liquid accumulation occurs above the plunger during shut-in. Alternative lift configurations such as bypass or continuous plunger systems may exhibit different pressure signatures that require modified interpretation.

Despite these limitations, the framework provides a scalable and computationally efficient method for extracting physically meaningful diagnostics from high-frequency plunger lift data.

VIII. Conclusions

High-frequency surface pressure measurements provide a valuable but often underutilized source of information for diagnosing plunger lift system behavior. This work demonstrates that by structuring these measurements at the cycle level, surface pressure data can be transformed into interpretable physical indicators describing hydraulic loading, plunger motion, and liquid delivery performance.

A deterministic diagnostic framework was developed that uses peak shut-in pressure differentials to infer retained hydraulic load and combines this information with plunger arrival timing and slug duration to estimate delivered liquid transport. From these quantities, a cycle-level lift efficiency index can be computed, allowing operators to monitor relative unloading performance over time. When analyzed together, retained load and delivery

efficiency provide a practical means of distinguishing between hydraulic retention failures, such as standing valve leakage, and mechanical issues such as plunger non-arrival.

Beyond the hydraulic diagnostics, this work introduces a hybrid edge–cloud architecture for reliable detection of plunger on-bottom events. A lightweight physics-based dynamic model embedded within the controller estimates plunger descent in real time by integrating tubing pressure measurements and simplified force balance relationships. This deterministic model removes reliance on transient pressure disturbances traditionally used for arrival detection and provides stable position estimates even when the pressure signal is weak or contaminated by noise.

To maintain model accuracy as well conditions evolve, a cloud-based adaptation layer performs probabilistic validation of on-bottom timing using Bayesian change-point detection and periodically re-optimizes model parameters using Bayesian optimization. This architecture separates real-time deterministic computation at the edge from computationally intensive statistical inference in the cloud, allowing the system to adapt to changing well conditions while preserving deterministic execution on embedded hardware.

Field deployment across more than 900 wells and validation on 50 representative wells demonstrate that the proposed approach significantly improves reliability of on-bottom detection compared with traditional pressure-transient methods while reducing the need for continuous manual tuning.

An important outcome of this work is the demonstration that modern plunger lift controllers capable of collecting high-frequency pressure measurements can serve as an instrumentation platform for multiple complementary analytical approaches. Within a single architecture, the same data stream supports deterministic physics-based state estimation, statistical change-point detection, and adaptive machine learning–based optimization workflows.

By enabling these complementary methodologies within a unified data and control framework, the approach establishes a scalable foundation for plunger lift diagnostics, health monitoring, and future closed-loop optimization across large well populations.

References

[1] W. Hearn, “Gas Well Deliquification,” in *Abu Dhabi International Petroleum Exhibition and Conference*, Abu Dhabi, UAE: SPE, Nov. 2010, p. SPE-138672-MS. doi: 10.2118/138672-MS.

[2] K. E. Brown, “Overview of Artificial Lift Systems,” *J. Pet. Technol.*, vol. 34, no. 10, pp. 2384–2396, Oct. 1982, doi: 10.2118/9979-PA.

[3] L. Rao, *Engineering mechanics: statics and dynamics*. New Delhi, India: Prentice-Hall of India, 2007.

[4] J. P. Brill, “Multiphase Flow in Wells,” *J. Pet. Technol.*, vol. 39, no. 01, pp. 15–21, Jan. 1987, doi: 10.2118/16242-PA.

[5] O. L. Rowlan, J. N. McCoy, and A. L. Podio, “Plunger Lift Analysis, Troubleshooting and Optimization,” in *Canadian International Petroleum Conference*, Calgary, Alberta: PETSOC, Jun. 2007, p. PETSOC-2007-159. doi: 10.2118/2007-159.

[6] J. F. Lea, “Dynamic Analysis of Plunger Lift Operations,” *J. Pet. Technol.*, vol. 34, no. 11, pp. 2617–2629, Nov. 1982, doi: 10.2118/10253-PA.

[7] G. M. Hashmi, A. R. Hasan, and C. S. Kabir, “Design of Plunger Lift for Gas Wells,” in *SPE North America Artificial Lift Conference and Exhibition*, The Woodlands, Texas, USA: SPE, Oct. 2016, p. D011S003R001. doi: 10.2118/181220-MS.

[8] E. S. Page, “Continuous Inspection Schemes,” *Biometrika*, vol. 41, no. 1/2, p. 100, Jun. 1954, doi: 10.2307/2333009.

[9] S. Aminikhanghahi and D. J. Cook, “A survey of methods for time series change point detection,” *Knowl. Inf. Syst.*, vol. 51, no. 2, pp. 339–367, May 2017, doi: 10.1007/s10115-016-0987-z.

[10] V. Chandola, A. Banerjee, and V. Kumar, “Anomaly detection: A survey,” *ACM Comput. Surv.*, vol. 41, no. 3, pp. 1–58, Jul. 2009, doi: 10.1145/1541880.1541882.

[11] P. I. Frazier, “A Tutorial on Bayesian Optimization,” 2018, *arXiv*. doi: 10.48550/ARXIV.1807.02811.

[12] S. Brooks, “Markov chain Monte Carlo method and its application,” *J. R. Stat. Soc. Ser. Stat.*, vol. 47, no. 1, pp. 69–100, Mar. 1998, doi: 10.1111/1467-9884.00117.

Table of Figures